A process-oriented model study of equatorial Pacific phytoplankton: the role of iron supply and tropical instability waves

M. Vichi [a,b,*] S. Masina [a,b] F. Nencioli [c,1]

[a]*Centro Euro-Mediterraneo per i Cambiamenti Climatici, Bologna, Italy*

[b]*Istituto Nazionale di Geofisica e Vulcanologia, Bologna, Italy*

[c]*Centro Interdipartimentale di Ricerca per le Scienze Ambientali, Ravenna, Italy*

Abstract

The response of phytoplankton growth to iron supply and its modulation by large scale circulation and tropical instability waves (TIWs) in the eastern equatorial Pacific has been investigated with an ocean biogeochemical model. This process study shows that iron can be efficiently advected from the New Guinea shelf through the Equatorial Undercurrent (EUC) to the eastern Pacific. The presence of a continental iron source is necessary for the maintenance of the observed subsurface iron maximum in the EUC core. In the eastern Pacific region, phytoplankton production is enhanced when additional iron is available in the EUC. Simulated phytoplankton variability is linked to TIWs activity, as revealed by a wavelet analysis of the total autotrophic carbon. The net local effect of the waves on phytoplankton can be either positive or negative depending on several factors. When the iron nutricline is sufficiently shallow to be reached by the wave vertical scale, the effect of the waves is to enhance iron availability in the euphotic zone leading to a net local increase of phytoplankton biomass. We therefore suggest that the local maxima of phytoplankton observed in moorings off the Equator in the eastern Pacific might be not only the result of

concentration mechanisms, but also the result of an increase in local production sustained by advected iron.

Key words: biogeochemical model, BFM, PELAGOS, tropical instability waves, iron, equatorial Pacific

---

1 Introduction

Dissolved bioavailable iron is a crucial regulator of the productive phase of marine phytoplankton in the eastern equatorial Pacific (Martin et al., 1994; Coale et al., 1996). However, it is still under debate which mechanisms control the supply of iron to the photic zone from the major geochemical sources (Johnson et al., 1997; Fung et al., 2000; Croot et al., 2007). Atmospheric deposition of mineral dusts is generally considered the main source for the global ocean (Tegen and Fung, 1994; Fung et al., 2000; Gao et al., 2003), while in the eastern Equatorial Pacific the dominant source to the euphotic zone is upwelling and mixing from the subsurface ocean (Christian et al., 2002). In other regions, inputs from the continental margins can supply comparable amounts of iron to the open ocean (Johnson et al., 1999; Elrod et al., 2004). Iron limitation is one of the mechanisms that are ascribed to control phytoplankton growth in the equatorial Pacific, together with excessive grazing (Landry et al., 1997) and silicate limitation (Dugdale and WIlkerson, 1998). The relatively low concentrations of surface $Si(OH)_4$ observed in the region may

* Marcello Vichi, CMCC, V. Aldo Moro 44, 40127 Bologna. +39 051 3782631 Fax: +39 051 3782654

   Email address: `vichi@bo.ingv.it` (M. Vichi).
   URL: `http://www.cmcc.it` (M. Vichi).
[1] now at Ocean Physics Laboratory, University of California at Santa Barbara, USA

specifically limit diatom growth (Dugdale and WIlkerson, 1998; Dugdale et al., 2007) due to reduced silicate supply with respect to preformed nitrate.

The discovery of elevated iron concentrations in the core of the Equatorial Undercurrent (EUC, Gordon et al., 1997; Landry et al., 1997) has pointed out the importance of this large-scale current in advecting iron to the eastern Pacific (Ryan et al., 2006). The origin of this maximum is attributable to the continental shelves surrounding northern New Guinea (Mackey et al., 2002) and it has been argued that the supply of iron through the EUC is consistently modulated by the phase of the El Niño Southern Oscillation (ENSO, Ryan et al., 2006).

The upwelling of iron-rich waters from the EUC is one of the major factors promoting phytoplankton production in the central and eastern equatorial Pacific (Gordon et al., 1997; Ryan et al., 2002, 2006). It is likely that any enhancement of upwelling into the euphotic zone could lead to additional biomass production. The IronEx experiment confirmed that iron limits production and development of larger phytoplankton cells in the eastern Pacific (Coale et al., 1996). In general, increases in productivity in this region (e.g., during the autumn EqPac cruises in 1992) were ascribed to increased iron inputs (Foley et al., 1997; Barber et al., 1996), although several other factors may modulate phytoplankton productivity at larger spatial scales.

Mesoscale processes in the equatorial Pacific such as tropical instability waves (TIWs) have been interpreted as being "analogous to a natural iron enrichment experiment" (Barber et al., 1996). The presence of TIWs is in fact associated to significant changes in the divergence of horizontal velocity and therefore to both upwelling and downwelling processes (Flament et al., 1996; Willett et al., 2006; Pennington et al., 2006). Downwelling characterizes the cold crest of a TIW at few degrees north of the equator, while upwelling occurs in the trough of the waves

3

close to the equator where warm water is advected from higher latitudes. Temporary iron inputs from the EUC have been ascribed to increases in vertical advection linked to the passage of upwelling Kelvin waves and TIWs (Foley et al., 1997; Barber et al., 1996), although direct measurements of increased iron concentrations still remain to be collected in order to confirm this hypothesis.

There are several documented cases of high chlorophyll concentration associated with TIWs (Yoder et al., 1994; Murray et al., 1994.; Foley et al., 1997; Chavez et al., 1998; Dunne et al., 2000; Strutton et al., 2001; Legeckis et al., 2004) . Estimated productivity has been observed up to 50% higher than climatological values (Foley et al., 1997). Blooms observed in 1998 around the Marquesas Islands, a region high in nutrients but poor in iron, have been attributed to southward pulses of cool and iron-rich upwelled waters of the EUC. Satellite images clearly shows that these elevated chlorophyll concentrations originate at the southern boundary of TIWs (Legeckis et al., 2004). Very high chlorophyll anomalies (an order of magnitude greater than the background concentration) have been observed in 1998 in coincidence with the passage of TIWs (Strutton et al., 2001). Some of the high-chlorophyll features observed during that experiment were probably formed by a subductive front that concentrated biomass as in the case of the "line in the sea" (Yoder et al., 1994) whereas others might have been induced by enhanced production as a result of enhanced nutrient flux to the euphotic zone.

Despite the growing consensus in the scientific community on the role of iron in the world ocean (e.g. Veldhuis and De Baar, 2005), there is still a systematic lack of data that prevents the construction of robust predictive models of phytoplankton variability in the equatorial Pacific. Climatological numerical experiments (Christian et al., 2002) have pointed out that iron modelling in the upper ocean is hampered by sparse information regarding sources, abundance and distribution of

iron, as well as by the limited knowledge of the relevant processes on the annual and inter-annual scales that affect iron concentrations and bioavailability in the euphotic zone. Nonetheless, models can still be successfully used to test hypotheses with process-oriented studies, which might also drive data collection strategies to reduce specific uncertainties in our understanding of the processes relevant to phytoplankton production. Several issues regarding the role of TIWs on nutrient fluxes in the equatorial eastern Pacific are still unresolved. Some authors suggest that the visible TIWs induced biomass enhancement is due to advection and convergence of biomass (Yoder et al., 1994), while others suggest that is local increase in primary production (Strutton et al., 2001). In contrast with the mooring observations, recent numerical studies (Gorgues et al., 2005) have shown that TIWs induce a decrease of both iron concentration and new production when the whole upwelling region of the equatorial Pacific is considered.

Regardless of the net effect that the waves have on the biological activity of the entire divergence region, a quantitative identification of the processes that make iron available in the eastern equatorial Pacific is still missing. In particular, we are interested in understanding how an iron source in the western Pacific can influence iron availability in the eastern Pacific and, as a consequence, the new production of the region. We have used a coupled ocean biogeochemical model to investigate some aspects of phytoplankton variability induced by changes in the large scale iron inventory in the EUC and by TIWs dynamics. The experiment and the diagnostics have been specifically designed to elucidate the role of these large scale and mesoscale mechanisms on phytoplankton dynamics, focusing on the eastern equatorial Pacific region.

Changes in the EUC iron inventory due to different external sources and the effects on phytoplankton on the TIW scale have been investigated by means of scenario

experiments. The "Control" simulation presented in this work is only driven by atmospheric iron deposition, while the "FeSource" run includes an additional source of iron parameterized as continental iron originating from the New Guinea shelf and advected by the EUC. The chosen investigation period was 1990-2001 which allowed the identification of several different periods of TIW activity and the interannual fluctuations of the large-scale upwelling due to the strong and modest events of ENSO found in this decade. In Sections 2.1 and 2.2 we describe the experiment design and model set up with particular emphasis on iron initialization. Section 3 contains results from a wavelet analysis used to correlate biomass variability with TIW dynamics and from other analyses of the experiments. Finally, in Section 4 we provide a discussion and summarize the main results.

2   Experiment design

2.1   Model description

The numerical model of the global ocean used in this study is PELAGOS (PELAgic biogeochemistry for Global Ocean Simulations, Vichi et al., 2007a,b). It is composed of a three dimensional ocean general circulation model (OGCM) based on OPA 8.2 (Madec et al., 1999), and the biogeochemistry model BFM (`http://bfm.cmcc.it`) derived and modified from the European Regional Seas Ecosystem Model (Baretta et al., 1995; Baretta-Bekker et al., 1997, ERSEM I/II). The OGCM has a resolution of $2°$ with a finer mesh of $0.5°$ of latitudes at the equator (Madec and Imbard, 1996), which allows to resolve the physical processes of interest to this study. The first level of the vertical grid is at 5 m, with a 10 m step in the top 150 m.

The physical model computes the advection and diffusion terms and provides the light and temperature fields for the calculation of the biogeochemical source terms. The system is fully-coupled as it also provides the instantaneous attenuation of the short-wave radiation penetrating the ocean interior related to biological processes. The biogeochemical model is fully detailed in Vichi et al. (2007b). It implements a set of biomass-based differential equations that describes the fluxes of carbon, nitrogen, phosphorus and silica among selected biological functional groups representing the major components of the lower trophic levels. The principal functional groups in the pelagic environment are represented by unicellular planktonic autotrophs (pico-, nano-phytoplankton and diatoms), zooplankton (nano-, micro- and meso-) and heterotrophic bacterioplankton. The model also simulates the dynamics of nitrate, ammonium, phosphate, biogenic silicate, oxygen and has an explicit parameterization of the biochemical cycling of dissolved/particulate non-living organic matter. In this specific experiment Fe uptake is parameterized differently as in Vichi et al. (2007b) by assuming a simple Michaelis-Menten kinetics with different saturation constants for each phytoplankton group. This choice was mostly driven by the availability of *in situ* iron enrichment experiments which provided a possible value of the half-saturation constant for the average phytoplankton population (Coale et al., 1996). The observed value of 0.1 μmol m^{-3} is set as representative of diatoms, while the values for nano and picophytoplankton are set an order of magnitude lower to indicate less limitation by this nutrient. As suggested by Christian et al. (2002), by using a Michaelis-Menten kinetics, the constant ratio of iron uptake with respect to the constituent representing the biomass (N in his case and C in the case of PELAGOS) becomes a key parameter. Since the focus of this work is on the equatorial Pacific, we have chosen the minimum ratio observed by Sunda and Huntsman (1995, 1997) (3 μmol Fe/mg C), which implies iron to be a known limiting factor of this region.

The model is forced by imposing daily surface fluxes of heat, water and momentum from the ERA-40 reanalyses (Uppala et al., 2005) over the period 1990-2001 and by relaxing the surface temperature to the Reynolds data set (Reynolds et al., 2002) with a weak coefficient (40 W m^{-2} K^{-1}; 60 days). All the other physical parameterizations are set as in Vichi et al. (2007a). The initial fields of the physical variables are derived from a physics-only simulation of the period 1958-1989 initialized with climatological temperature and salinity data (Levitus et al., 1998).

2.2 *External iron sources and biogeochemistry initialization*

Atmospheric iron deposition is taken into account as done in Moore et al. (2002) by applying climatological model data from Tegen and Fung (1994) and assuming a dissolution fraction of 1%. Iron biogeochemistry is rather simplified: no organic ligands are considered; iron is remineralized at a constant rate from organic detritus produced by plankton (about a factor 10 less than hypothesized by Landry et al. (1997)); and it is slowly scavenged to sinking particles according to a parameterization proposed by Johnson et al. (1997) and also applied by Aumont et al. (2003) (cf. Vichi et al., 2007b).

A continental source of iron has been parameterized by imposing an iron profile observed on the shelf at about 2.5°S 146°E (Mackey et al., 2002) to the grid points belonging to the New Guinea shelf. The location of the source and the imposed profile are shown in Fig. 1. This procedure assumes a stationary source of iron over the entire continental shelf, thus neglecting any temporal and spatial variability. In particular, the shelf processes that originated such profiles as discussed by Mackey et al. (2002) are not considered in the model. Another important assumption concerns the bioavailability of the observed iron profile. The model does not consider

any effect of ligands and/or siderophores (e.g. Archer and Johnson, 2000; Kraemer, 2004) therefore all the iron prescribed on the continental shelf is available for phytoplankton growth.

All the biological functional groups are initialized with low homogeneous values and initial nutrient fields are derived from the World Ocean Atlas (Conkright et al., 2002) as presented in Vichi et al. (2007a). Iron was initialized with the homogeneous value of 0.6 μmol m^{-3}, which is quickly consumed during the spin-up time in the upper productive layers.

Both the Control and the FeSource experiments started from the same initial conditions derived from a 2 year spin-up climatological simulation with the iron source on the New Guinea shelf. This implies that the initial iron conditions in the equatorial Pacific are proper of a situation in which both the continental iron source and atmospheric deposition are present. In the FeSource experiment this source is maintained during the whole simulation period, while it is removed in the Control.

3 Model results

3.1 *Iron variability*

Fig. 1 illustrates the mean annual velocity and pattern of the simulated EUC at 182 m water depth, which is the average location of the EUC core in the western Pacific. The physical model can reproduce a realistic representation of the currents that feed the EUC from the New Guinea shelf. It thus provides the necessary mechanism for the advection of continental iron into the EUC as suggested by Mackey et al. (2002). A spin-up time of 2 years with climatological forcings was sufficient to

9

allow the advection of dissolved iron from the western source region to the central and eastern Pacific via the EUC.

The simulated inter-annual variability of the EUC and iron advection is shown in Fig. 2 as mass and iron transport at 140°W over the first 300 m. Fig. 2a agrees well with reconstructed TAO array data from Izumo (2005) over the same section and time period, indicating an adequate simulation of the EUC time evolution by the model. Transport-weighted iron concentration (Fig. 2b) is computed by normalizing the iron transport by the mass transport for the Control and FeSource experiments. The figure shows the adjustment of the Control experiment due to the removal of the continental source used in the spin-up phase. This trend is mostly visible in the western, deeper part of the basin and it has little effect on the phytoplankton biomass in the eastern upwelling zone (see Sec. 3.2). The FeSource scenario is stable throughout the simulation with a higher variability in the Fe transport with respect to the Control.

The inter-annual change of total biologically-available iron is further illustrated in Figs. 3 and 4. Figure 3 shows the Hovmöller diagram of simulated equatorial dissolved iron at the surface and at 182 m depth. This depth is well below the photic zone and no biological utilization is present. The eastward advection across the Pacific at 182 m is visible until 140°W (Fig 2b). Further East of 140°W the EUC shoals and iron concentration surface maxima are found (Fig. 3a). The iron upwelled at the Equator is then advected westward by the South Equatorial Current. Phytoplankton chlorophyll maxima are found in the same regions where dissolved iron is available (not shown). During the 1997-98 ENSO event there is no iron at the surface in the whole equatorial Pacific, and the maximum in the core of the EUC is limited to 180°E. In late winter 1997-98, the intensification of the EUC transport and upwelling leads to an initial increase of surface iron at 180°E (Fig.3a) and

10

eventually to the large upwelling from 160 to 120°W during the 1998 La Niña. A similar response is found in the observations of chlorophyll concentration as documented by Ryan et al. (2002, 2006).

The vertical location of the simulated iron maximum is shown in Fig. 4 together with the zonal velocity fields from the Control and FeSource experiments at 140°W. The initial conditions characterized by a maximum located slightly below the EUC core at 100 m are only maintained in the presence of the continental source of iron. In the Control experiment the initial maximum gradually decreases during the course of the experiment and is almost completely depleted by the end of the simulation period.

Fig. 5 shows a comparison between vertical profiles of iron from different years for both the Control and the FeSource experiment, and the real data collected by Coale et al. (1996) during JGOFS and provided electronically by Gregg et al. (2003). Both experiments are characterized by a realistic vertical distribution of iron, showing a subsurface increase around 150 m of depth. In the case of the Control experiment, the absence of a continental source of iron leads to a progressive disappearance of the iron maximum below the euphotic zone; on the other hand, iron concentrations remain fairly stable throughout the whole FeSource experiment and match the observed vertical distribution at 0°N, 140°W (Gordon et al., 1997). While the Control experiment shows values of irons that are comparable with the observed range of data, Fe concentrations in the FeSource experiment are approximately twice the observed values (Gordon et al., 1997). This indicates that the simple parameterization of the iron source applied in the model might represent a possible upper limit for the iron availability from the continental source. Despite being not completely realistic, the FeSource experiment is still valid in a process-oriented study. In fact, it provides a scenario with different conditions in terms of iron availability

to be compared with the Control experiment in order to understand the processes through which TIWs regulate iron availability in the eastern equatorial Pacific.

3.2   TIWs and phytoplankton dynamics

The physical characteristics of the TIWs simulated by the model are realistic both in terms of their spatial distribution and propagation features (Willett et al., 2006). A wavelet analysis of the meridional velocity indicates that both period (Fig. 6) and wavelength of the waves are in agreement with the observed values (Kennan and Flament, 2000; Legeckis et al., 2002; Willett et al., 2006). The wavelet analysis is a common tool in geophysical fluid dynamics. It is used to investigate events associated with undulatory phenomena (Torrence and Compo, 1998) and is particularly powerful in the identification of TIWs (e.g. Masina and Philander, 1999). The seasonal and interannual variability of the simulated TIWs are also realistic: in general the waves are present from the beginning of the boreal summer to December and are much more intense during La Niña years such as in 1998 (Fig. 6). In some years the period at 2°N (Fig. 6b) demonstrates a double peak suggesting that at this latitude the wavelet analysis may capture a mixed signal coming from two distinct waves (Lyman et al., 2007). Figure 7 demonstrates that the simulated chlorophyll is distributed along the TIW undulations observed in the sea surface temperature field (SST). These patterns are visually comparable with satellite observations (e.g. Willett et al., 2006). The spatial distribution of chlorophyll is similar in both experiments, although the average concentrations are higher in the FeSource experiment (Fig. 7c versus Fig. 7a). The simulated iron distribution tends to be localized around the equator and it does not follow the northward wave fluctuations, particularly in the Control experiment where iron concentrations are lower and confined to the

eastern part of the model domain (Figs. 7b and 7d).

A region roughly corresponding to half the longitudinal extension of a tropical in-
stability wave (0-5°N, 118-122°W, Fig. 7c) was used to analyze the local effects
of TIWs on phytoplankton dynamics. Our analysis is focused on the northern re-
gion of the eastern equatorial Pacific because this is the region where the phys-
ical characteristics of the TIWs have been studied in more detail. Due to a well
defined temperature front between the North Equatorial Counter Current (NECC)
and the South Equatorial Current (SEC), this is also the region where the contrast
between the northward advection of cold, equatorial water and the southward ad-
vection of warmer tropical water is more pronounced. Therefore the biological pro-
cesses might be strongly affected by the physical processes associated with TIWs.
The northward extension of the box was set to 5¡N in order to capture the waves
in their entirety even during those years (such as 1998) when the front between the
NECC and the SEC was further displaced North due to a more intense equatorial
upwelling.

Phytoplankton carbon biomass was averaged in the box volume down to 100 m
depth, and the resulting time series for both the Control and the FeSource simula-
tions are shown in Figure 8a and b. The visual comparison of Fig. 8a and b clearly
indicates that changes in the absolute values of iron advected by the EUC lead to
an enhancement of the mean phytoplankton biomass in the target region.

The observed inter-annual variability in autotrophic biomass is due to both the
large-scale signal and the TIW modulation. In order to assess the actual role of
TIWs, we decided to remove the variability associated with time scales longer than
intraseasonal from the total signal. The total standing carbon stock have been fil-
tered by removing the 6 months running mean also depicted in Fig. 8. The residu-

13

als have been used to compute the wavelet power spectrum (Torrence and Compo, 1998), which is shown in Fig. 8c only for the FeSource experiment and limited to time scales typical for TIWs. The local variability of phytoplankton biomass is characterized by undulatory features with a period of 20-35 days occurring mostly in the period August-November, and characterized by wavelengths (not shown) that are also comparable with the ones typical of the TIWs (Flament et al., 1996; Masina and Philander, 1999). The comparison with the wavelet analysis of the meridional velocity anomaly in the same region (Fig. 6) confirms that the variability observed in phytoplankton biomass is tightly related to the TIWs phenomenon.

A key question is whether TIWs have a local net effect on phytoplankton biomass by effectively enhancing Fe availability. To answer this question we identified the periods of TIWs activity by selecting the time windows where the scale-averaged power spectrum of the 20-35 days component of the meridional velocity anomaly is significant (Fig. 9). TIW energy is considered significant when it is above the 95% significance level according to Torrence and Compo (1998). Note that the period of activity is not always confined within the same calendar year (e.g. 1999-2000). By convention, we take the starting date of the TIW period as indicator of the year. Year 2000 TIWs are not considered further in our analysis given the doubtful significance of the wave energy and the occurrence in the spring of 2001.

To separate the contribution of the wave-induced enhancement in phytoplankton production from the large-scale upwelling and seasonal variability we removed the longer-term average standing stock. The mean local change of total phytoplankton carbon during TIW activity for each year is thus defined as:

$$\Delta C_{TIW} = \frac{100}{\Delta T_{TIW}} \int\limits_{\Delta T_{TIW}} \frac{C - C_r}{C_r} dt \qquad (1)$$

14

where C is the timeseries of total phytoplankton carbon in the box, C_r the 6-month running average and ΔT_{TIW} the period of the year where TIWs are significantly energetic as identified in Fig. 9. The choice of the 6-month window is related to the fact that the waves are phase locked with the annual cycle and that some of their effects are likely to be seen at lower frequencies. It is important to remark that the results discussed here are robust to the reduction of the averaging window down to the monthly time scale (not shown), although the local ΔC_{TIW} is reduced, indicating that part of the signals come from lower frequency processes.

The results are plotted for both simulations in Fig. 10a. In addition Fig. 10b shows the depth of the Fe nutricline and a proxy of the TIW vertical scale, both averaged over the same time window ΔT_{TIW}. The chosen proxy is the meridionally-averaged depth of the vertical velocity maxima at 120°W. between 0 and 3°N where both the equatorial and TIW-induced upwelling is found. This meridional average was chosen in order to capture the interannual changes in the wave characteristics as further shown in Fig. 11.

The periods when TIWs were active are characterized by different net biomass responses, indicating that TIWs do not always enhance phytoplankton production. The FeSource run has always larger positive (lower negative) ΔC_{TIW} due to the additional continental Fe supply to the EUC which enhances phytoplankton carbon production. This is a robust response of the model mostly caused by the permanent iron-limiting average conditions in the surface ocean. Interestingly, despite the variations in phytoplankton biomass shows a strong inter-annual variability in both experiments, Control and FeSource experiments are characterized by positive (negative) responses during the same years.

Fig. 10b suggests that the relative location of the nutricline with respect to the ver-

tical extension of TIWs can help to interpret the net increase/decrease of biomass. When the TIW vertical scale is sufficiently deeper than the nutricline, the contribution of TIWs, either via upwelling and/or meridional advection, can provide sufficient amounts of iron to further enhance net phytoplankton production. On the other hand, when the two vertical scales are comparable, the downwelling feature of TIWs and/or their equatorial advection of iron-poor waters are likely to dominate. It is also possible that this effect prevails if the role of TIWs is averaged over the whole divergence region as suggested by the model results of Gorgues et al. (2005). Favorable conditions were met in 1992, 1995, 1996, 1999 but not in the other years. The 1998 La Niña is an exception because the values of the TIW and nutricline scales are comparable, yet the change in biomass is positive.

The yearly variability in the vertical scales of TIWs is better clarified in Fig. 11, where the 120°W section of vertical velocity averaged over the TIW periods is plotted together with the nutricline and the depth of the 20 $°C$ isotherm. In 1992, which is an example of net biomass increase, the TIW contribution directly affects the location of the Fe nutricline, which is shallower in the upwelling part and deeper in the downwelling. In 1993, vertical velocities are smaller than in 1992 indicating that the waves are weaker. Also, the large scale upwelling is weaker as shown by the deeper 20 $°C$ isotherm. The maxima of vertical velocities are found above the nutricline and thus the wave is not capable to further increase phytoplankton production with respect to the long-term average. Finally, 1998 is characterized by a shallow thermocline and nutricline at the Equator and the TIW vertical scale of activity is confined close to the surface. The waves are active as evidenced by an increase with respect to the mean biomass concentration (Fig. 10a). However, in these conditions, TIWs are unlikely to directly affect the nutricline depth since the effects of the large scale upwelling are dominant.

To further analyze the direct effect of the waves in advecting Fe in different years, we computed the wave-driven iron fluxes $\langle V \prime Fe \prime \rangle_{TIW}$ and $\langle W \prime Fe \prime \rangle_{TIW}$, where

$$V \prime = V - V_r \tag{2}$$
$$W \prime = W - W_r \tag{3}$$
$$Fe \prime = Fe - Fe_r \tag{4}$$

are the residual meridional and vertical velocities and iron concentration after the removal of the 6-month running means (V_r, W_r, Fe_r) and $\langle \cdot \rangle_{TIW}$ indicates the average over the TIW period.. Since iron is not a passive tracer in the model but is consumed by phytoplankton while being advected, the concentration used in this computation is the residual of both physical and biological processes acting at the time scales of the TIWs. Fig. 12 shows the wave-driven fluxes computed at the same section as in Fig. 11 for two selected years (1992 and 1993). Meridional fluxes are higher than vertical fluxes in all the analyzed years, with positive values in the euphotic zone when TIWs lead to a net enhancement of phytoplankton biomass (e.g. 1992, see also Fig. 10a), and negative values (as in 1993) when there is a net decrease in biomass associated with the wave.

The analysis of the vertical wave-driven fluxes also hints at the existence of wave-driven upwelling as evidenced by the positive values both in 1992 and 1993. In 1992, when the waves lead to a net increase in biomass, it is evident the signature of iron upwelling at the equator and iron downwelling further north. On the other hand, in 1993, there is a weaker and almost uniform upwelling localized across the nutricline (Fig. 12).

In Fig. 13 and 14 we plot the time series at 2°N, 120°W of vertical velocity, meridional velocity, total phytoplankton carbon and dissolved iron from the FeSource experiment averaged over the uppermost 100m for years 1992 and 1993, respectively.

17

While Fig. 10 and 11 describe the integrated effect of the wave over different years, the time series help us to understand the instantaneous processes acting during the passage of the wave. This picture clearly shows that the peaks in phytoplankton carbon and dissolved iron coincide with downwelling of northward advected cold water in the edge of the wave as found in the observations (e.g. Strutton et al., 2001). Vice-versa, during the passage of the wave trough, when there is upwelling of warm water directed toward the equator, both phytoplankton carbon and dissolved iron amounts decrease. The wave has thus a three-dimensional structure that needs to be carefully considered and may complicate the interpretation of local variability. We suggest that in cases of enhanced productivity during TIW activity such as in 1992, an extra source of iron was made available at the equator by upwelling processes due to large scale and wave activity. The iron was not completely consumed locally and was advected northward by the wave to iron-limited regions where it can trigger local production during the downwelling phase of the wave. (This hypothesis is further analyzed in the following Section with a specific study case). In 1993 when TIWs are also present but their effect on phytoplankton production is negative, wave induced variability is clearly seen in total phytoplankton carbon but not in dissolved iron. This suggests that there is no northward advection of iron from the equatorial region, due most likely to upwelling of shallower, iron-poor waters. The role of TIWs in this case is simply to advect and redistribute phytoplankton. Year 1993 is indeed an example of one of the years when the iron nutricline at the equator (see Fig. 10 and 11) is particularly deep and the vertical scale of the waves is too shallow to effectively upwell iron-rich waters.

3.3 Year 1992: a case study

Our analysis suggests that the effect of TIWs depends on the depth of the iron nu-
tricline relative to the vertical scale of the waves. It is because of this that TIWs not
always induce an increase of phytoplankton production. However, even in cases
when TIWs effectively induce a net phytoplankton enhancement it is still unclear
whether TIWs simply advect biomass produced at the equator (Legeckis et al.,
2004), where chlorophyll maxima are always present even during weak ENSO pe-
riods (Foley et al., 1997), or instead they induce a net local phytoplankton increase.
To answer this question we analyze in detail one of the years when the TIW-induced
effect on phytoplankton is positive. Fig. 15 shows the simulated time series for year
1992 of total phytoplankton carbon, dissolved iron and total primary production av-
eraged over the first 100 m at 0°N, 120°W for both experiments. At this latitude the
amount of total phytoplankton carbon and its temporal variability are very similar in
both experiments. From the time series of primary production it is evident that both
cases are particularly productive during the second half of the year in connection
with the large scale upwelling due to the intensification of the trade winds. At the
equator, this process is dominant and the presence of TIWs is not clearly detectable
in the time series. The Control experiment reaches a productivity peak during the
boreal summer and then decays. The FeSource experiment maintains a high pro-
ductivity level up to November and then rapidly decreases. Overall it is interesting
to note that the productivity of the two experiments does not differ much even if the
availability of iron at the equator is much greater in the FeSource experiment with
respect to the Control (Fig. 15b). This is a consequence of the Michaelis-Menten
form of phytoplankton growth, indicating that the equatorial Fe concentration is
above the half-saturation concentration in both experiments.

19

The same quantities from Fig. 15 are shown in Fig. 16 at 2°N. At this latitude, the time variability of both the total phytoplankton carbon and primary production is dominated by mesoscale variability due to the presence of the TIWs in the second half of the year. In both experiments, the passage of a wave results in an increase of up to 100% in total phytoplankton carbon with respect to the background level. At the same time the peaks of total phytoplankton carbon are higher in the FeSource experiment and reach values up to 50% higher than in the Control experiment. The physics is exactly the same in the two experiments and the biomass concentration at the equator is very similar (Fig. 15a). If the mechanisms in action at 2°N were simply advection and convergence of phytoplankton biomass due to the waves, the total phytoplankton carbon should be similar in both cases. We believe that the waves do not simply advect phytoplankton produced elsewhere but can induce increased local production. This conclusion is supported by the time series of primary production at 2°N (Fig. 16c), which clearly shows that the phytoplankton blooms during TIW activity during the FeSource experiment are always associated with enhancement in primary production. During phytoplankton blooms the primary production increases up to an order of magnitude in the FeSource experiment. Despite the fact that iron availability at the equator is significantly different in the two experiments, iron concentrations at 2°N are more similar on average throughout the period (Fig. 16b). This suggests that the extra supply of iron advected by the EUC in the eastern Pacific and upwelled at the equator mainly by the large scale dynamics (but also by the TIW-induced vertical fluxes, cf. Fig. 12) has been utilized during the northward advection by the TIW. Only small amounts of unused Fe remain at this latitude. On the contrary, in the Control experiment only the first two blooms are correlated with enhanced primary productivity, suggesting that when iron is the limiting nutrient TIWs are acting mainly to advect and converge biomass produced in other regions.

20

4 Discussion and conclusions

The ocean biogeochemical model used in this work is not primarily meant to predict the evolution of the equatorial Pacific ecosystem, but rather to approximate the major processes and to deduce cause-effect mechanisms controlling the phytoplankton variability. The specific model design shows that substantial iron concentrations can be advected from the New Guinea shelf through the EUC, to the upwelling regions of the central and eastern Pacific as hypothesized by Mackey et al. (2002). Iron is utilized in small quantities during this process because the EUC is below the photic zone. Our process study demonstrates that the presence of a continental iron source is necessary for the maintenance of the subsurface iron maximum in the EUC core observed by Gordon et al. (1997).

However, the rather simplistic parameterization of iron source used in this study does not account for the spatial and temporal variability in continental iron supply, both of which might have some effects on the absolute value of iron concentrations. If, on the one hand, the application of a distant source partly solves the problems presented by Christian et al. (2002), where their model was sensitive to the choice of the imposed initial concentration profile in the core of the EUC, on the other, major concerns remain on the assumption of bioavailability of the measured iron profile that was chosen as representative of the shelf condition. In fact, in our experiment all the iron measured in the profile was assumed to be available to phytoplankton growth without considering any possible effect of ligands (e.g. Archer and Johnson, 2000). This assumption provides an upper limit for continental iron availability in the eastern Pacific and it needs to be further investigated to obtain more realistic simulations. The simulated concentrations in the central equatorial Pacific are highly influenced by the values imposed on the shelf, however even the

simplified profile used in this study allows for values comparable with the observed ranges (Coale et al., 1996; Gordon et al., 1997). This process study clearly indicates that further iron supply to the central and eastern Pacific due to the inclusion of a continental source and subsequent advection through the EUC, leads to enhanced biomass compared to a simulation where only atmospheric deposition is imposed.

The model results are in agreement with the field-work analyses of Coale et al. (1996), Foley et al. (1997) and Strutton et al. (2001) regarding the iron transport in the EUC and the local effects of TIWs on phytoplankton biomass. Both the presence of TIWs and variations in the sources of iron to the EUC do have an effect on phytoplankton. The model is able to simulate realistic TIWs in terms of period and wavelength, and there is a clear relation between the periods of TIWs activity and phytoplankton carbon variability.

The analysis of selected periods when TIWs are active has shown that in some cases TIWs can be an efficient mechanism for increasing phytoplankton carbon production. However, their effect is superimposed on the large-scale upwelling and is linked to the depth of the iron nutricline. The processes that determine this depth are not only limited to equatorial Ekman pumping. It has been shown that in some years (e.g. 1992) the iron nutricline can be vertically displaced underby the action of the TIWs. When the nutricline is sufficiently shallow and/or the TIWs vertical scale is deeper than the nutricline depth, TIWs contribute directly to the net increase of biomass by enhancing iron availability in the euphotic zone. Further investigations are needed to explore the linkages between TIWs and the depth of the iron nutricline, which is likely to be connected both to the uptake/regeneration of iron in the euphotic zone and to the large-scale equatorial upwelling. In particular, the choice of the iron parameterization in the modeled biogeochemistry can have a direct role and should be further assessed by conducting sensitivity studies

with different formulations (e.g. the Droop-like iron limitation used in Vichi et al. (2007b)).

The difference between the Control and the FeSource experiments is maximal during periods of TIW activity. In particular, they differ in biomass north of the equator on the western edge of the wave characterized by northward transport and downwelling of cold waters. In cases when the net effect of TIWs on phytoplankton is positive, such as in 1992, phytoplankton blooms at $2°N$ are correlated with dissolved iron maxima. This suggests that portion of the iron upwelled near the equator is not consumed locally. This iron can then be advected northward by the TIWs, thus "fertilizing" iron-poor regions and increasing phytoplankton biomass north of the equator. This conclusion is supported by the analysis of the iron fluxes induced by TIWs and by the fact that the phytoplankton blooms at $2°N$ are well correlated with peaks of primary productivity that reach values up to an order of magnitude higher than the background level. Our findings suggest that the waves have a differential effect on Fe availability in the eastern equatorial Pacific, which likely depends on the amount of iron in the EUC core and on the characteristics of the wave. In years when TIWs are weak (in terms of their upwelling and downwelling contribution) and their vertical scale is not deep enough to reach the nutricline, the meridional wave-driven Fe fluxes are negative and while phytoplankton blooms are still evident at $2°N$ the presence of TIWs do not induce a net phytoplankton increase. In these cases the effect of TIWs is simply a redistribution and advection of biomass in iron-poor waters. This mechanism partly explains why other modelling results (e.g. Gorgues et al., 2005) reported a negative effect of TIWs on the mean phytoplankton biomass and iron inventory. Our interpretation suggests that the average influence of TIWs is linked to the characteristics of the modeled waves which are in turn related to the variability of the large-scale upwelling during the chosen

23

simulation period.

The potential role of iron supply on phytoplankton growth should further be investigated in conjunction with silicate availability, since it has been shown that Si:N and Si:P ratios in phytoplankton change in iron depleted conditions (Takeda, 1998). PELAGOS assumes a constant Si:C ratio in diatoms which is typical of temperate regions and is lower than the values found in the equatorial Pacific and Southern Ocean (Vichi et al., 2007b). This is probably the major reason why PELAGOS overestimate silicate concentrations in the eastern equatorial Pacific (see Vichi et al., 2007a). Further sensitivity experiments similar to the one performed by Chai et al. (2007) needs to be performed to elucidate the co-limitation processes at work in the HNLC regions (e.g. Veldhuis and De Baar, 2005). It is nevertheless important to remark that the modulation by TIWs investigated in this work might affect the distribution of silicate as well, as pointed out by Dugdale et al. (2007).

The effects of large-scale and mesoscale processes on the equatorial Pacific phytoplankton are difficult to separate and our analysis is an attempt to reconcile the different aspects inferred from observations and modelling exercises. Our results indicate that this kind of ocean biogeochemical model is capable of capturing the basic mechanisms, and to explain the combined action of iron availability from distance sources and the modulation by mesoscale processes. However, the lack of qualitative and quantitative data on iron variability in connection with phytoplankton functional types prevents a direct validation of the model and the assessment of predictive skills. On the other hand, the understanding of the simulated processes increases our degree of confidence in describing modifications of the equatorial Pacific ecosystem due to climate change.

Acknowledgements

References

Archer, D. E., Johnson K. S., , 2000. A model of the iron cycle in the ocean. Glob. Biogeochem. Cy. 14, 269–279.

Aumont, O., Maier-Reimer, E., Monfray, P., Blain, S., 2003. An ecosystem model of the global ocean including Fe, Si, P co-limitations. Glob. Biogeochem. Cy. 17 (2), 1060.

Barber, R., Sanderson, M., Lindley, S., Chai, F., Newton, J., Trees, C., Foley, D., Chavez, F., 1996. Primary productivity and its regulation in the equatorial pacific during and following the 1991-1992 el nino. Deep-Sea Res. Pt. II 43, 933–969.

Baretta, J., Ebenhöh, W., Ruardij, P., 1995. The European Regional Seas Ecosystem Model, a complex marine ecosystem model. J. Sea Res. 33 (3-4), 233–246.

Baretta-Bekker, J., Baretta, J., Ebenhoeh, W., 1997. Microbial dynamics in the marine ecosystem model ERSEM II with decoupled carbon assimilation and nutrient uptake. J. Sea Res. 38 (3/4), 195–212.

Chavez, F., Strutton, P., Mcphaden, M. J., 1998. Biological-physical coupling in the central equatorial Pacific during the onset of the 1997-98 el niño. Geophys. Res. Lett. 25, 3543–3546.

Chai F., Jiang, M.-S. , Chao, Y., Dugdale, R. C., Chavez, F., Barber, R. T., 2007.

Modeling responses of diatom productivity and biogenic silica export to iron enrichment in the equatorial Pacific ocean. Glob. Biogeochem. Cy., 21, GB3S90, doi:10.1029/2006GB002804.

Christian, J. R., Verschell, M. A., Murtugudde, R., Busalacchi, A. J., McClain, C. R., 2002. Biogeochemical modelling of the tropical Pacific Ocean. II: Iron biogeochemistry. Deep-Sea Res. Pt. II 49, 545–565.

Coale, K. H., Fitzwater, S. E., Gordon, R. M., Johnson, K. S., Barber, R. T., 1996. Control of community growth and export production by upwelled iron in the equatorial Pacific ocean. Nature 379, 621–624.

Conkright, M., Garcia, H., O'Brien, T., Locarnini, R., Boyer, T., Stephens, C., Antonov, J., 2002. World Ocean Atlas 2001, Volume 4: Nutrients. Vol. NOAA Atlas NESDIS 52. U.S. Government Printing Office, Washington D.C., cD-ROMs.
URL http://www.nodc.noaa.gov/OC5/WOA01/woa01v4d.pdf

Croot, P. L., Frew, R. D., Sander, S., Hunter, K. A., Ellwood, M. J., Pickmere, S. E., Abraham, E. R., Law, C. S., Smith, M. J., Boyd, P. W., 2007. Physical mixing effects on iron biogeochemical cycling: Fecycle experiment. J. Geophys. Res. 112, C06015.

Dunne, J. P., Murray, J. W., Rodier, M., Hansell, D. A., 2000. Export flux in the western and central equatorial Pacific: zonal and temporal variability. Deep-Sea Res. Pt. I 47, 901–936.

Dugdale, R. C., and F. P. Wilkerson, 1998, Silicate regulation of new production in the equatorial Pacific upwelling, Nature, 391, 270 Ð 273

Dugdale, R. C., Wilkerson, F. P., Chai, F., Feely, R., 2007. Size-fractionated nitrogen uptake measurements in the equatorial Pacific and confirmation of the low Si–high-nitrate low-chlorophyll condition. Glob. Biogeochem. Cy. 21, GB2005, doi:10.1029/2006GB002722.

Elrod, V. A., Berelson, W. M., Coale, K. H., Johnson, K. S., 2004. The flux of iron from continental shelf sediments: A missing source for global budgets. Geophys. Res. Lett. 31, L12307.

Flament, P., Kennan, S. C., Knox, R. A., Niiler, P. P., Bernstein, R. L., 1996. The three-dimensional structure of an upper ocean vortex in the tropical Pacific ocean. Nature 383, 610–613.

Foley, D. G., Dickey, T. D., Mcphaden, M. J., Bidigare, R. R., Lewis, M. R., Barber, R. T., Lindley, S. T., Garside, C., Manov, D. V., Mcneil, J. D., 1997. Longwaves and primary productivity variations in the equatorial Pacific at 0°, 140^oW. Deep-Sea Res. Pt. II 44 (9-10), 1801–1826.

Fung, I. Y., Meyn, S. K., Tegen, I., Doney, S. C., John, J. G., Bishop, J. K. B., 2000. Iron supply and demand in the upper ocean. Glob. Biogeochem. Cy. 14, 281–295.

Gao, Y., Fan, S. M., Sarmiento, J. L., 2003. Aeolian iron input to the ocean through precipitation scavenging: A modeling perspective and its implication for natural iron fertilization in the ocean. J. Geophys. Res.-atmos 108, 4221.

Gordon, R. M., Coale, K. H., Johnson, K. S., 1997. Iron distributions in the equatorial Pacific: Implications for new production. Limnol. Oceanogr. 42, 419–431.

Gorgues, T., Menkes, C., Aumont, O., Vialard, J., Dandonneau, Y., Bopp, L., 2005. Biogeochemical impact of tropical instability waves in the equatorial Pacific. Geophys. Res. Lett. 32, L24615.

Gregg, W. W., Ginoux, P., Schopf, P. S., Casey, N. W., 2003. Phytoplankton and iron: validation of a global three-dimensional ocean biogeochemical model. Deep-Sea Res. Pt. II 50, 3143–3169.

Johnson, K. S., Chavez, F. P., Friederich, G. E., 1999. Continental-shelf sediment as a primary source of iron for coastal phytoplankton. Nature 398, 697–700.

Johnson, K. S., Gordon, R. M., Coale, K. H., 1997. What controls dissolved iron

concentrations in the world ocean? Mar. Chem. 57, 137–161.

Kennan, S. C., Flament, P. J., 2000. Observations of a tropical instability vortex. J. Phys. Oceanogr. 30 (9), 2277–2301.

Kraemer, S. M. 2004. Iron oxide dissolution and solubility in the presence of siderophores. Aquatic Sci. 66, 3–18.

Izumo, T., 2005. The equatorial undercurrent, meridional overturning circulation, and their roles in mass and heat exchanges during El Niño events in the tropical Pacific Ocean. Oc. Dynam., 55 (2), 110–123

Landry, M. R., Barber, R. T., Bidigare, R. R., Chai, F., Coale, K. H., Dam, H. G., Lewis, M. R., Lindley, S. T., Mccarthy, J. J., Roman, M. R., Stoecker, D. K., Verity, P. G., White, J. R., 1997. Iron and grazing constraints on primary production in the central equatorial Pacific: An EqPac synthesis. Limnol. Oceanogr. 42, 405–418.

Legeckis, R., Brown, C., Chang, P. S., 2002. Geostationary satellites reveal motions of ocean surface fronts. J. Mar. Sys. 37 (1-3), 3–15.

Legeckis, R., Brown, C. W., Bonjean, F., Johnson, E. S., 2004. The influence of tropical instability waves on phytoplankton blooms in the wake of the Marquesas Islands during 1998 and on the currents observed during the drift of the Kon-Tiki in 1947. Geophys. Res. Lett. 31.

Levitus, S., Boyer, T., Conkright, M., O'Brien, T., Antonov, J., Stephens, C., Stathoplos, L., Johnson, D., Gelfeld, R., 1998. WORLD OCEAN DATABASE 1998: Vol. 1: Introduction. Vol. NOAA Atlas NESDIS 18. U.S. Gov. Printing Office, Washington D.C.

Lyman, J.M., Johnson, G. C., Kessler, W. S., 2007. Distinct 17-day and 33-day tropical instability waves in subsurface observations. J. Phys. Oceanogr. 37, 855–872.

Mackey, D. J., O'sullivan, J. E., Watson, R. J., 2002. Iron in the western Pacific: a

riverine or hydrothermal source for iron in the Equatorial undercurrent? Deep-Sea Res. Pt. II 49, 877–893.

Madec, G., Delecluse, P., Imbard, M., Levy, C., February 1999. OPA8.1 ocean general circulation model reference manual. Notes du pole de modelisation, IPSL, France, http://www.lodyc.jussieu.fr/opa.

URL `http://www.lodyc.jussieu.fr/opa`

Madec, G., Imbard, M., 1996. A global ocean mesh to overcome the North Pole singularity. Clim. Dynam. 12, 381–388.

Martin, J. H., Coale, K. H., Johnson, K. S., Fitzwater, S. E., Gordon, R. M., Tanner, S. J., Hunter, C. N., Elrod, V. A., Nowicki, J. L., Coley, T. L., Barber, R. T., Lindley, S., Watson, A. J., Vanscoy, K., Law, C. S., Liddicoat, M. I., Ling, R., Stanton, T., Stockel, J., Collins, C., Anderson, A., Bidigare, R., Ondrusek, M., Latasa, M., Millero, F. J., Lee, K., Yao, W., Zhang, J. Z., Friederich, G., Sakamoto, C., Chavez, F., Buck, K., Kolber, Z., Greene, R., Falkowski, P., Chisholm, S. W., Hoge, F., Swift, R., Yungel, J., Turner, S., Nightingale, P., Hatton, A., Liss, P., Tindale, N. W., 1994. Testing the iron hypothesis in ecosystems of the equatorial Pacific Ocean. Nature 371, 123–129.

Masina, S., Philander, S. G. H., 1999. An analysis of tropical instability waves in a numerical model of the Pacific Ocean. Part 1: Spatial variability of the waves. J. Geophys. Res. 104 (C12), 29613–29635.

Moore, J. K., Doney, S. C., Glover, D. M., Fung, I. Y., 2002. Iron cycling and nutrient-limitation patterns in surface waters of the World ocean. Deep-Sea Res. Pt. II 49, 463–507.

Murray, J. M., Barber, R. T., Roman, M. R., Bacon, M. P., Feely, R. A., 1994. Physical and biological controls on carbon cycling in the equatorial Pacific. Science 266, 58–65.

Pennington, J., Mahoney, K., Kuwahara, V., Kolber, D., Calienes, R., Chavez,

F., 2006. Primary production in the eastern tropical pacific: a review. Prog. Oceanogr. 69, 285–317.

Reynolds, R. W., Rayner, N. A., Smith, T. M., Stokes, D. C., Wang, W., 2002. An improved in situ and satellite SST analysis for climate. J. Climate 15 (13), 1609–1625.

Ryan, J. P., Polito, P. S., Strutton, P. G., Chavez, F. P., 2002. Unusual large-scale phytoplankton blooms in the equatorial Pacific. Prog. Oceanogr. 55, 263–285.

Ryan, J. P., Ueki, I., Chao, Y., Zhang, H., Polito, P. S., Chavez, F. P., 2006. Western pacific modulation of large phytoplankton blooms in the central and eastern equatorial pacific phytoplankton blooms in the central and eastern equatorial pacific. J. Geophys. Res. 111, G02013.

Strutton, P. J., Ryan, J. P., Chavez, F. P., 2001. Enhanced chlorophyll associated with tropical instability waves in the equatorial Pacific. Geophys. Res. Lett. 28 (10), 2005–2008.

Sunda, W. G., Huntsman, S. A., 1995. Iron uptake and growth limitation in oceanic and coastal phytoplankton. Mar. Chem. 50, 189–206.

Sunda, W. G., Huntsman, S. A., 1997. Interrelated influence of iron, light and cell size on marine phytoplankton growth. Nature 390, 389–392.

Takeda, S, 1998. Influence of iron availability on nutrient consumption ratio of diatoms in oceanic waters. Nature, 393, 774–777, doi:10.1038/31674.

Tegen, I., Fung, I., 1994. Modeling of mineral dust in the atmosphere - sources, transport, and optical-thickness. J. Geophys. Res.-atmos 99, 22897–22914.

Torrence, C., Compo, G. P., 1998. A practical guide to wavelet analysis. B. Am. Meteorol. Soc. 79, 61–78.

Uppala, S., Kallberg, P., Simmons, A., Andrae, U., da Costa Bechtold, V., Fiorino, M., Gibson, J., Haseler, J., Hernandez, A., Kelly, G., Li, X., Onogi, K., Saarinen, S., Sokka, N., Allan, R., Andersson, E., Arpe, K., Balmaseda, M., Beljaars, A.,

van de Berg, L., Bidlot, J., Bormann, N., Caires, S., Chevallier, F., Dethof, A., Dragosavac, M., Fisher, M., Fuentes, M., Hagemann, S., Holm, E., Hoskins, B., Isaksen, L., Janssen, P., Jenne, R., McNally, A., Mahfouf, J.-F., Morcrette, J.-J., Rayner, N., Saunders, R., Simon, P., Sterl, A., Trenberth, K., Untch, A., Vasiljevic, D., Viterbo, P., Woollen, J., 2005. The era-40 re-analysis. Quart. J. Roy. Meteor. Soc., 2961–3012.

Veldhuis, M., De Baar, H. J. W., 2005. Iron resources and oceanic nutrients: advancement of global environment simulations. J. Sea Res. 53, 1–6.

Vichi, M., Masina, S., Navarra, A., 2007a. A generalized model of pelagic biogeochemistry for the global ocean ecosystem. Part II: numerical simulations. J. Mar. Sys. 64, 110–134.

Vichi, M., Pinardi, N., Masina, S., 2007b. A generalized model of pelagic biogeochemistry for the global ocean ecosystem. Part I: theory. J. Mar. Sys. 64, 89–109.

Willett, C. S., Leben, R. R., Lavin, M. F., 2006. Eddies and tropical instability waves in the eastern tropical Pacific: A review. Prog. Oceanogr. 60, 218–238.

Yoder, J. A., Ackleson, S. G., Barber, R. T., Flament, P., Balch, W. M., 1994. A line in the sea. Nature 371, 689–692.
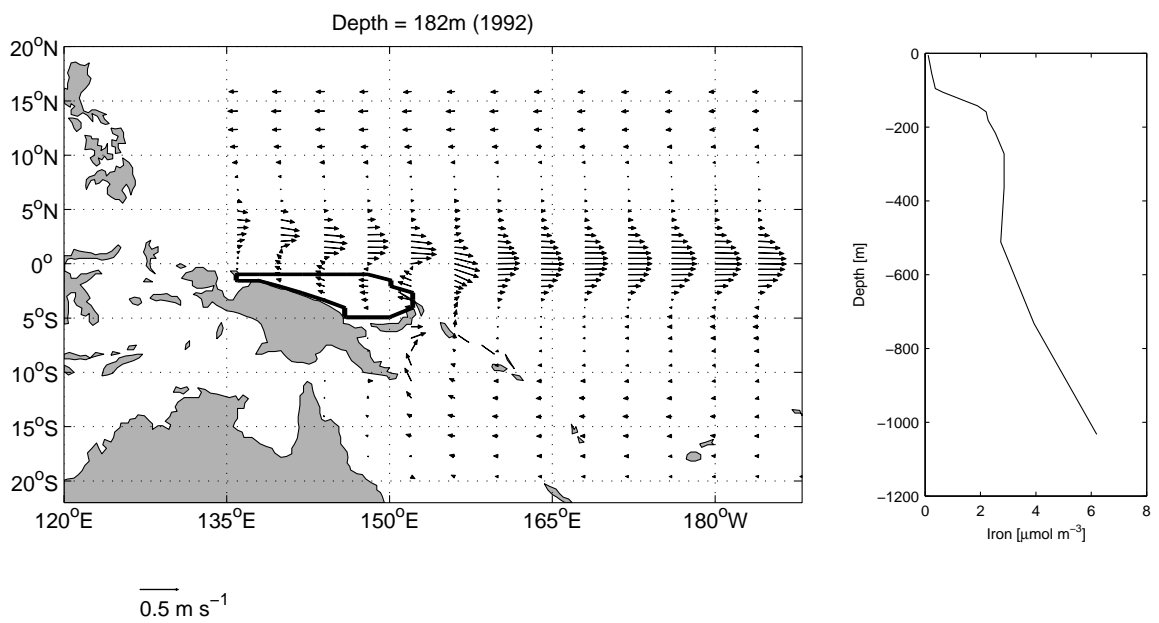
Figure 1. Mean simulated annual currents (year 1992) at the depth of the EUC and location of the New Guinea shelf where the iron vertical profile on the right (Mackey et al., 2002) is prescribed.
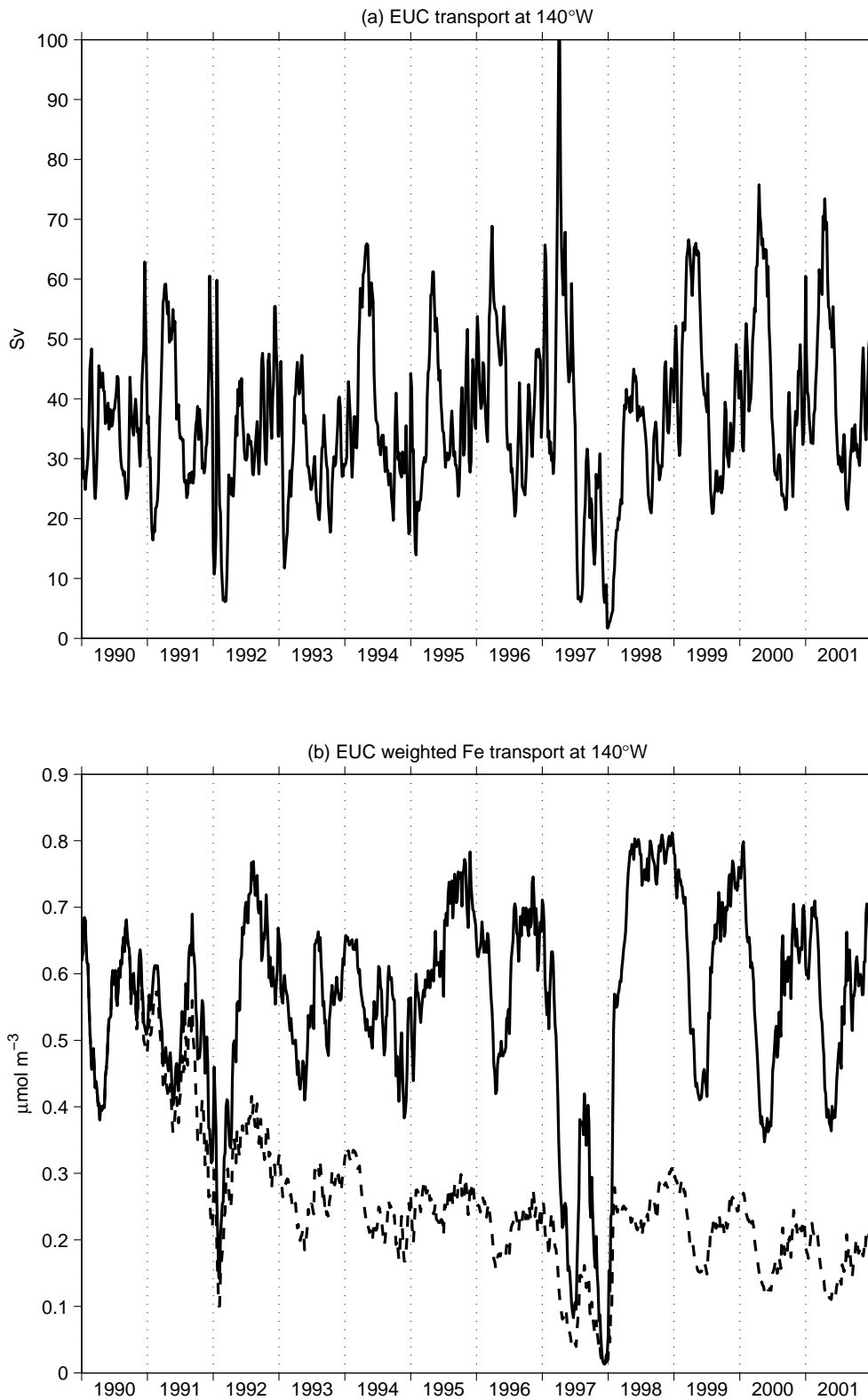
Figure 2. (a) Mass transport in the first 300 m at 140°W, 1°S-1°N and (b) transport-weighted iron concentration of EUC at 140°W from the FeSource (continuous line) and Control (dashed line) experiments.
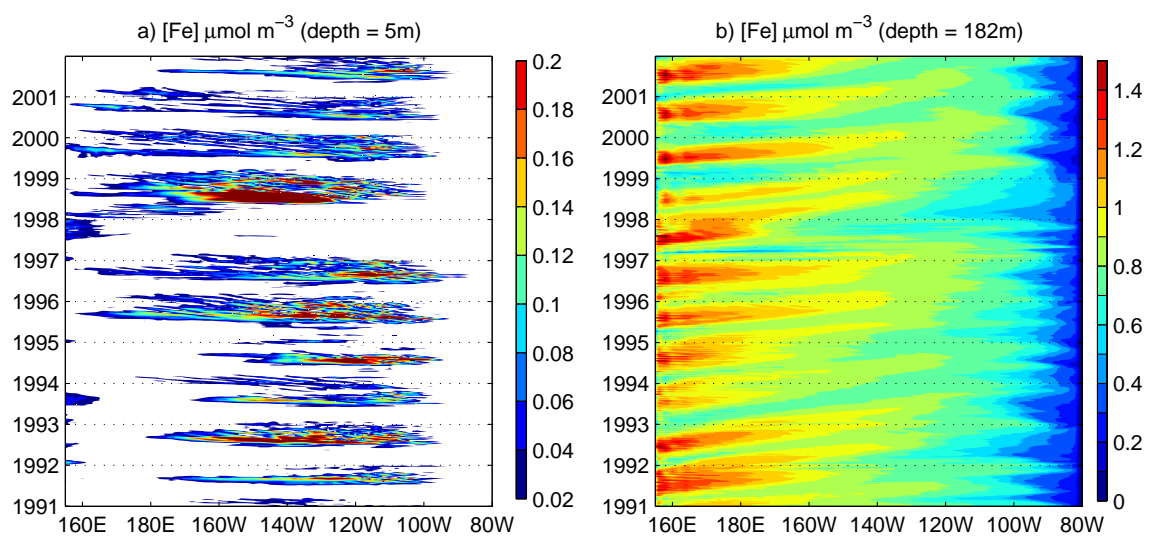
Figure 3. Hovmöller diagram at the equator of the simulated iron concentration at the surface and 182 m depth from the FeSource run (μmol m^{-3}).
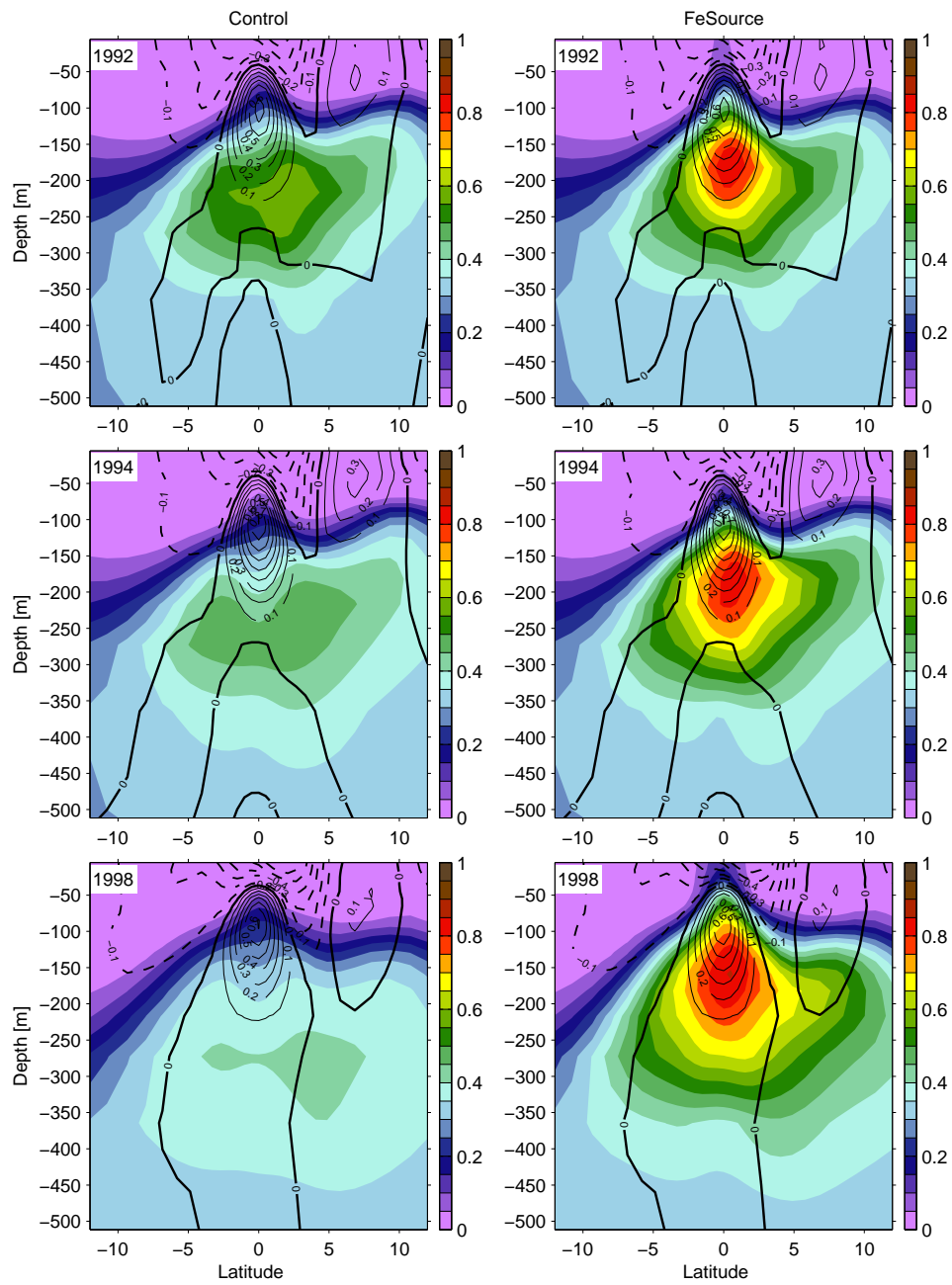
Figure 4. Mean annual concentrations for 1992, 1994 and 1998 of dissolved iron (shaded, μmol m^{-3}) and mean zonal velocity (contours, m s^{-1}) at 140°W for the Control (left panels) and FeSource (right panels) experiments
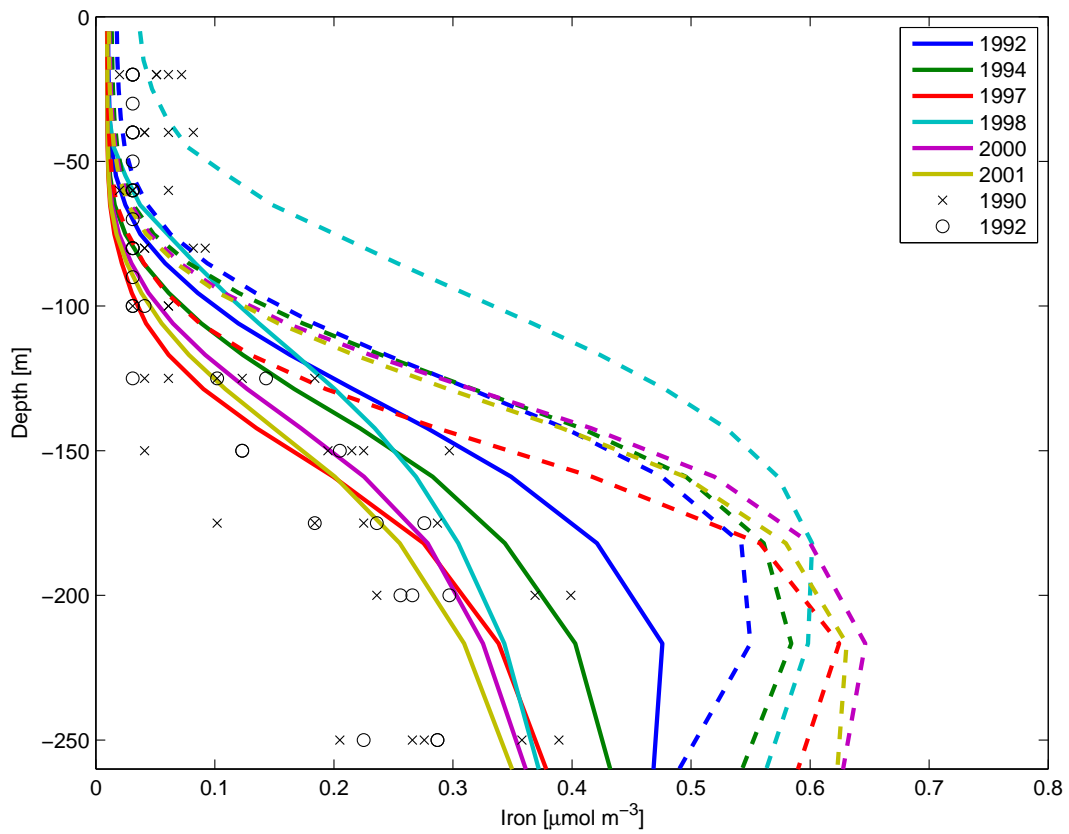
Figure 5. Comparison between mean annual iron concentration profiles from the Control (continuous lines) and FeSource (dashed lines) experiments (averaged at 9°S-9°N,140°W) and observations collected on a section at the same longitude (Coale et al., 1996).
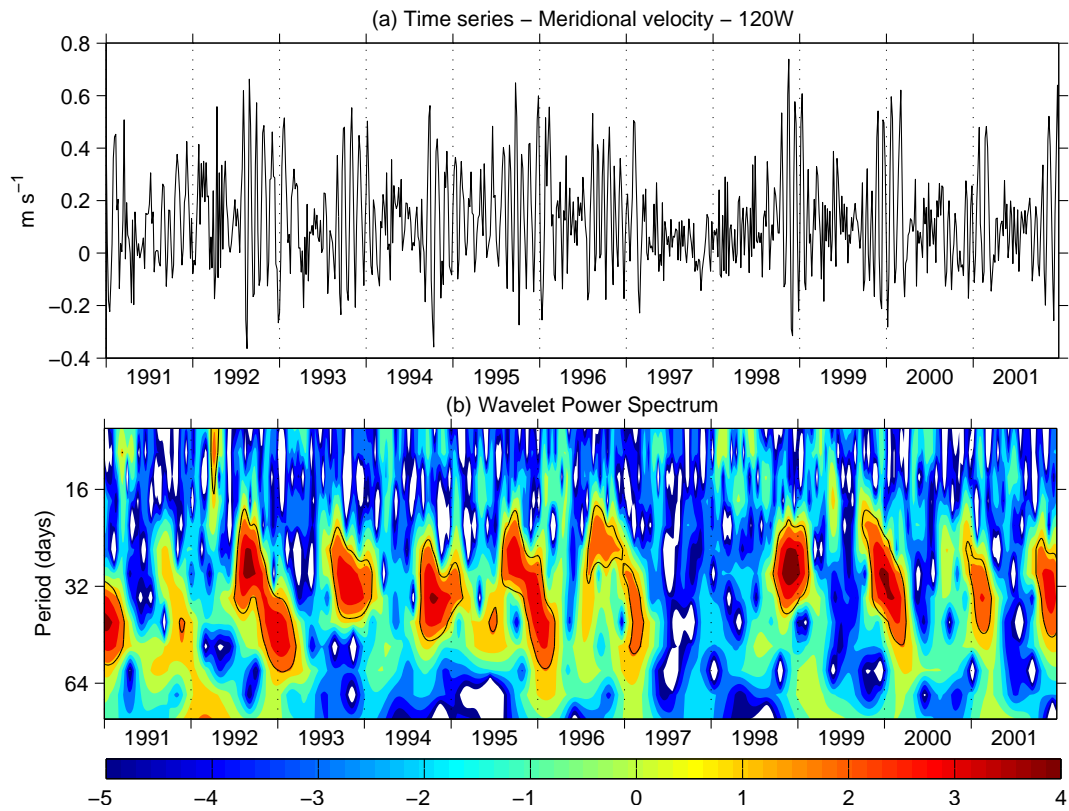
Figure 6. a) Timeseries of the meridional velocity at 2°N, 120°W and b) wavelet power spectrum with the 95% significance level according to Torrence and Compo (1998).
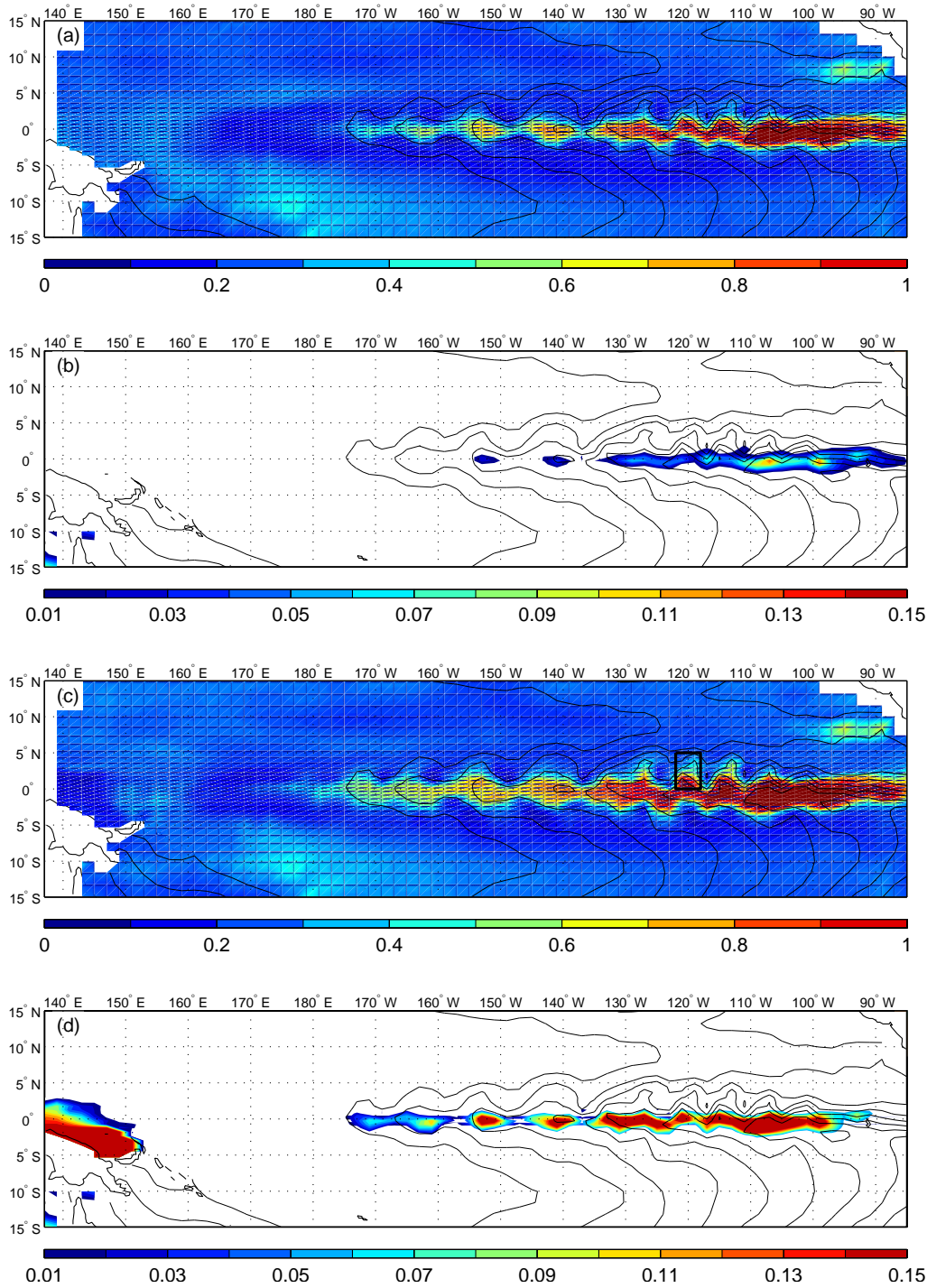
Figure 7. Snapshot (September 20, 1992) of the chlorophyll (mg m^{-3}) and iron (μmol m^{-3}) concentration averaged over the first 50 m for the Control (panels a and b) and Fesource (panels c and d) experiments. Temperature contours from 20 to 28 °C are superimposed. Panel c also shows the location of the region where the wavelet analysis was applied.
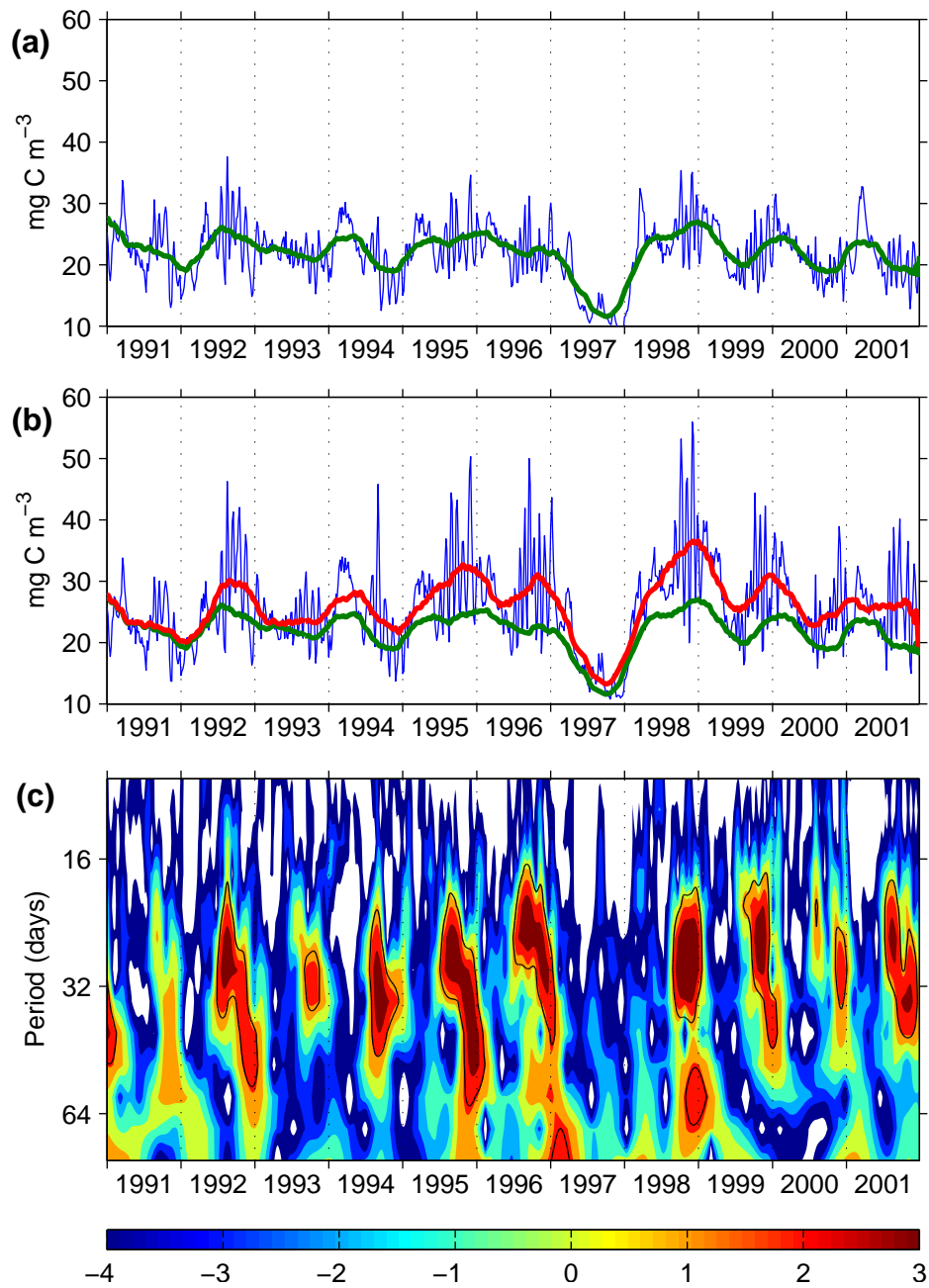
Figure 8. Phytoplankton biomass concentration in the target box and 6 month running means for (a) the Control run and (b) the FeSource run (the Control running mean in green is reported for direct comparison). (c) Wavelet power spectrum of the residuals with respect to the running mean for the FeSource experiment.
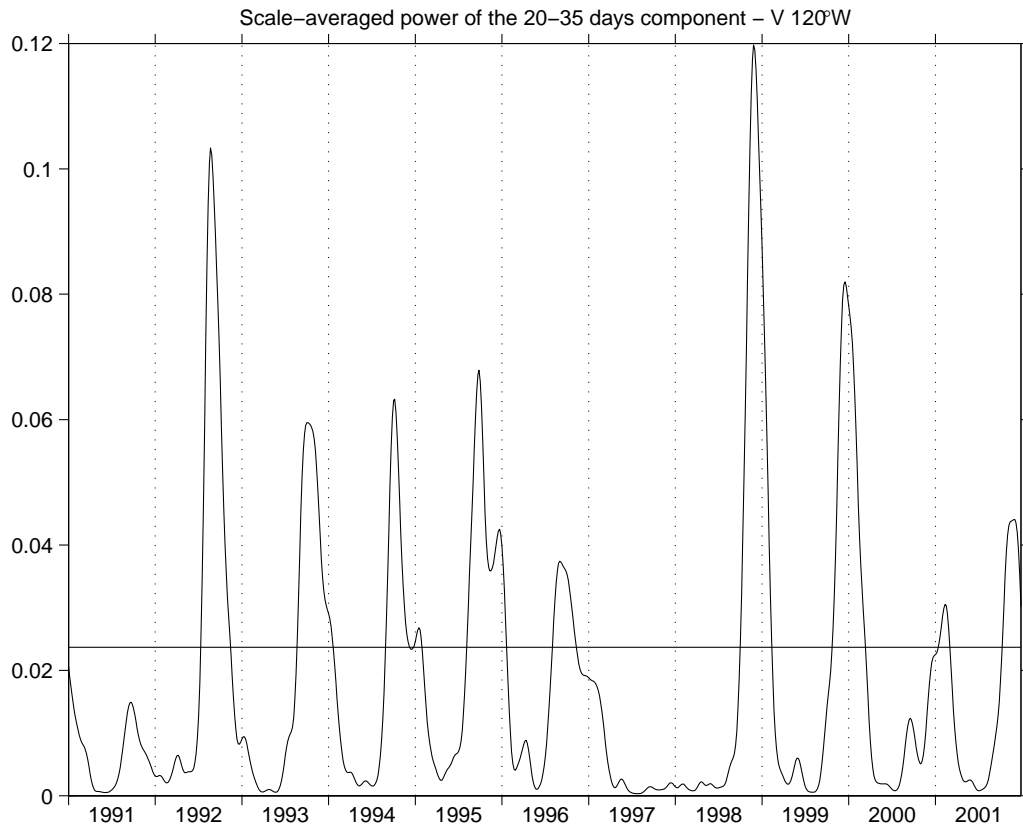
Figure 9. Scale-averaged power of the 20-35 days wavelet components of the meridional velocity at 120°W. The periods where TIWs are considered significant are the time-intervals where the power is above the reference line of 95% confidence level (Torrence and Compo, 1998).
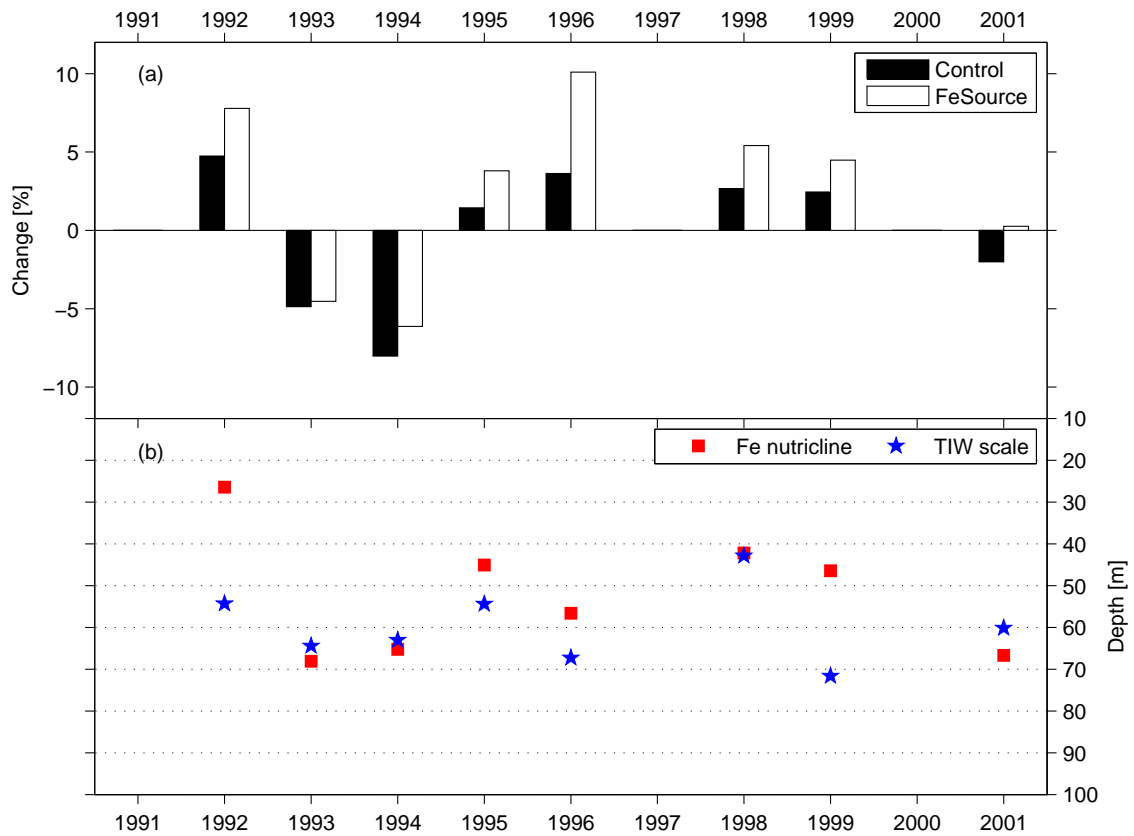
Figure 10. (a) mean percentage of biomass change in the box at 120°W and (b) mean depths of the Fe nutricline and estimate of the TIWs vertical scale (FeSource experiment only) during the periods of activity (see Fig. 9).
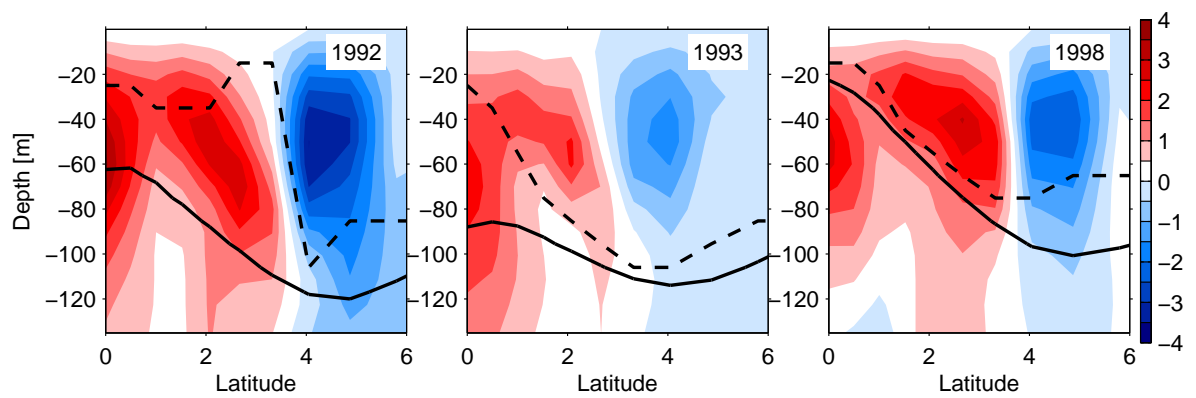
Figure 11. Meridional section at 120°W of vertical velocity (in m d^{-1}) averaged over the periods of TIWs activity in 1992, 1993 and 1998 (see Fig. 9). The depths of the 20 °C isotherm (continuous line) and of the Fe nutricline (dashed line) are superimposed (model data from the FeSource experiment).
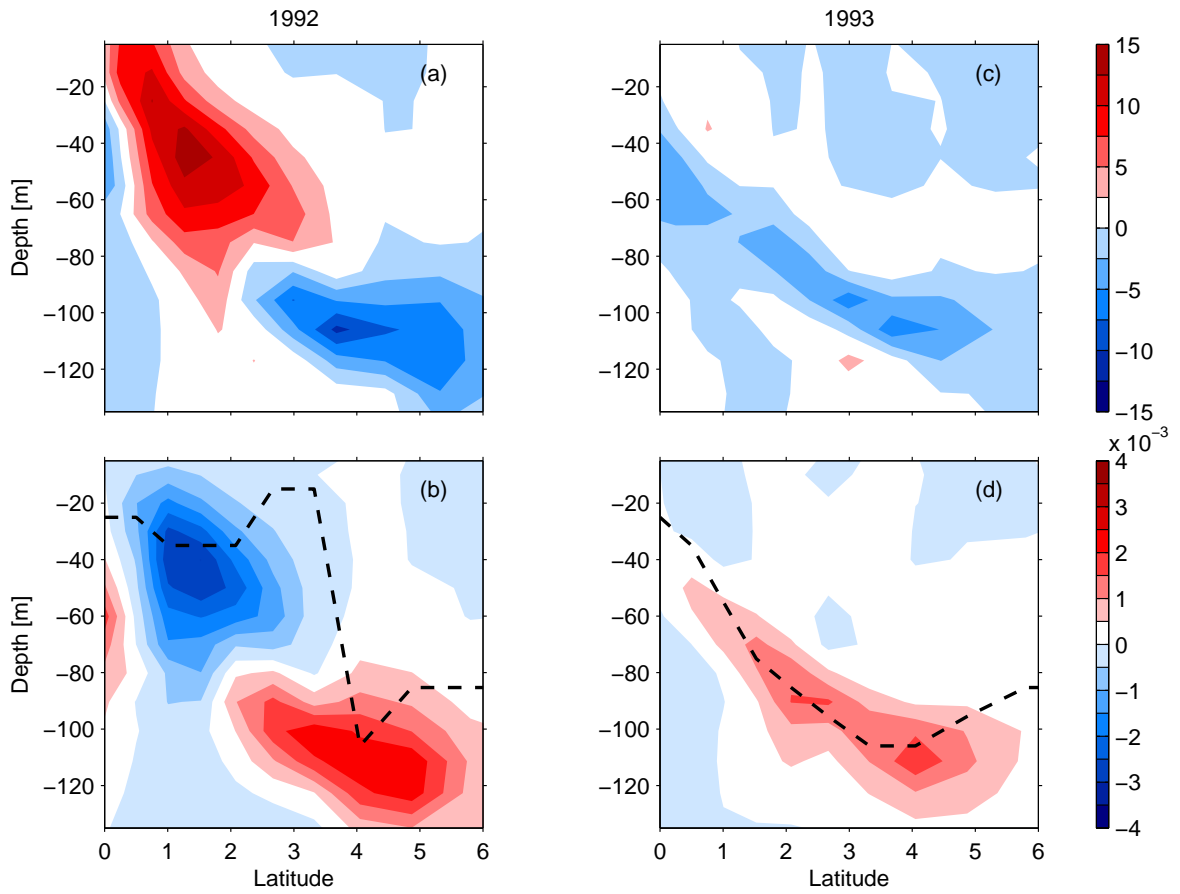
Figure 12. Meridional section at $120°$W of TIW-induced iron fluxes. (a) and (c) meridional fluxes; (b) and (d) vertical fluxes, in nmol Fe m^{-2} s^{-1}, averaged over the periods of TIWs activity in 1992 and 1993 (see Fig. 9).
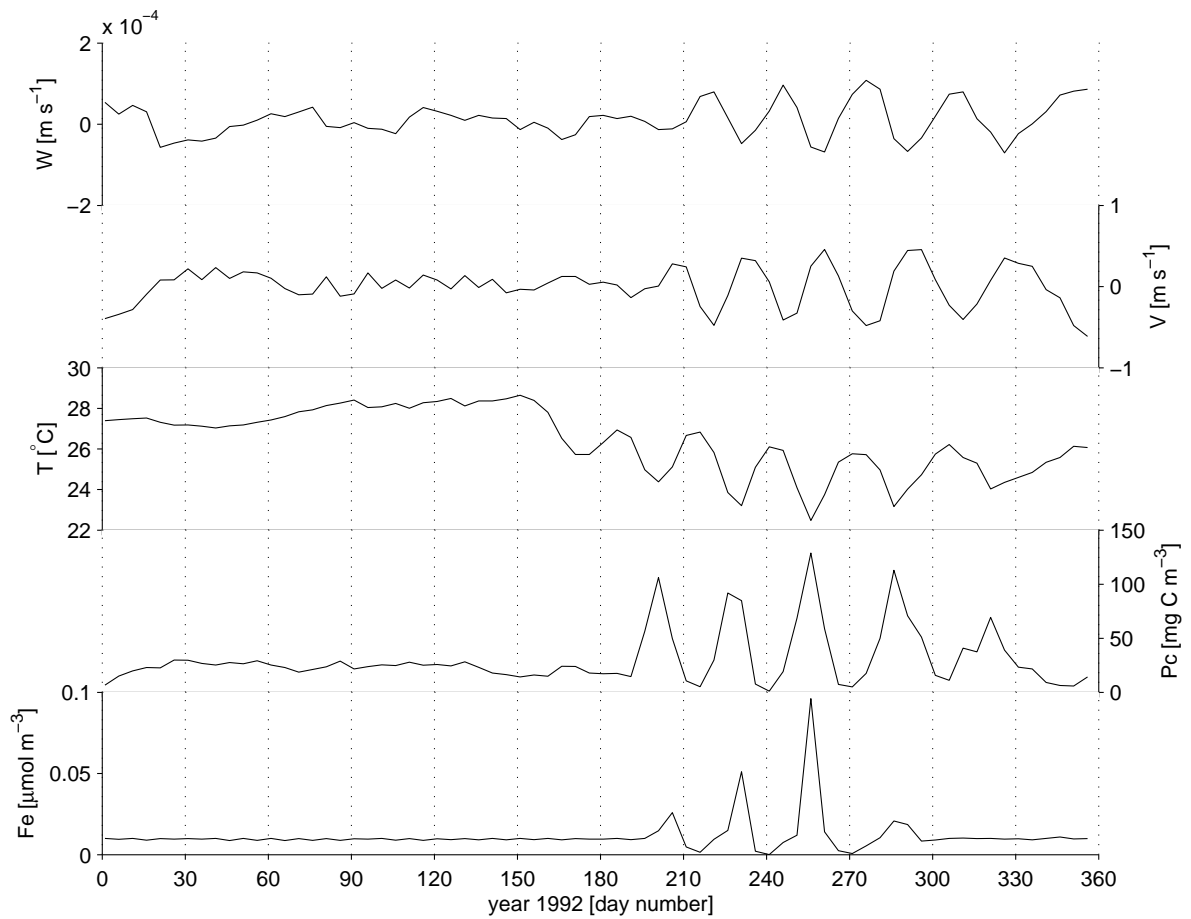
Figure 13. Simulated timeseries at 2°N, 120°W of vertical velocity, meridional velocity, temperature, total phytoplankton carbon and dissolved iron for year 1992, averaged over the first 100 m.
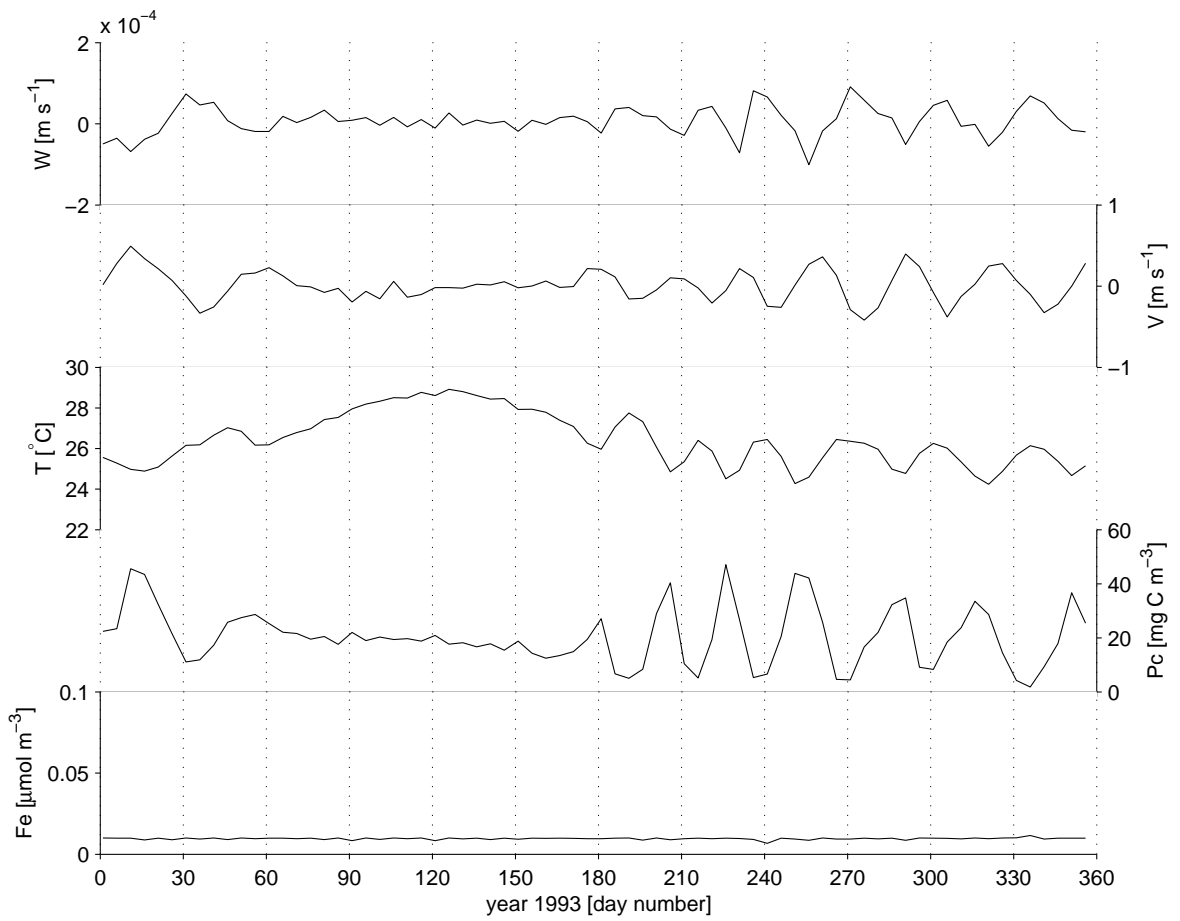
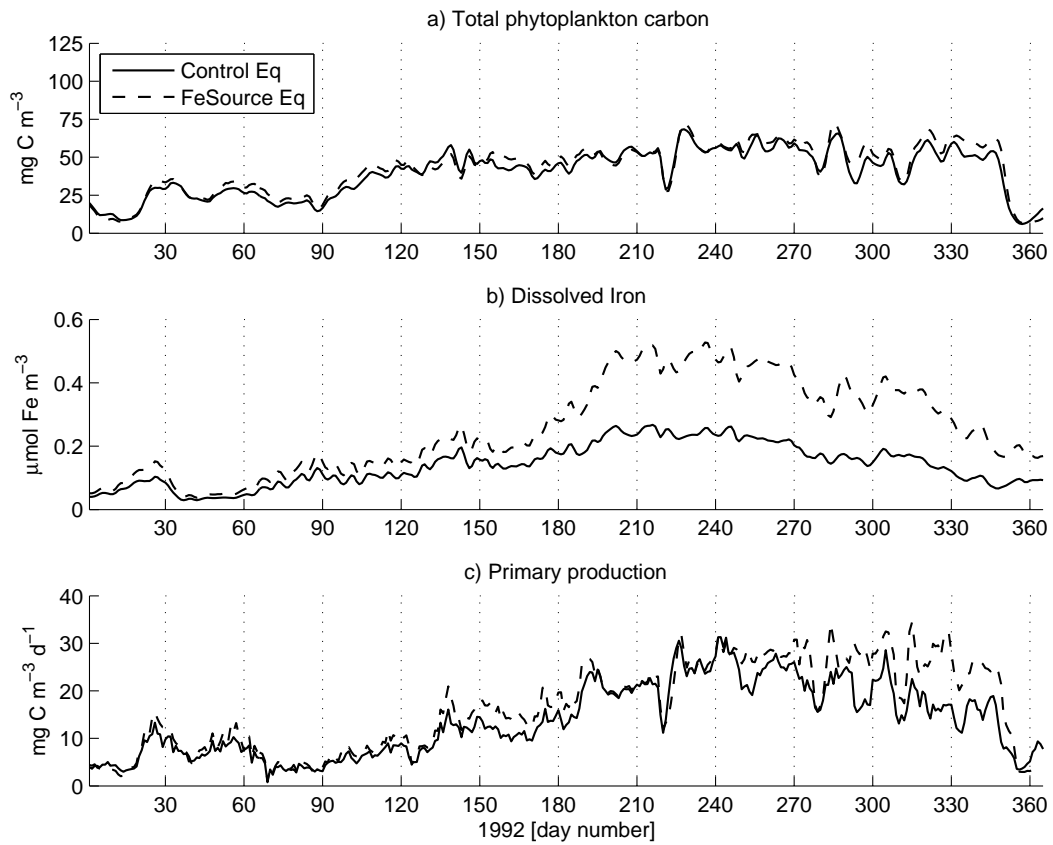Figure 14. Same as Fig. 13 but for year 1993.

Figure 15. Simulated timeseries at 0°N, 120°W of a) total phytoplankton carbon, b) dissolved iron and c) total primary production averaged over the first 100 m.
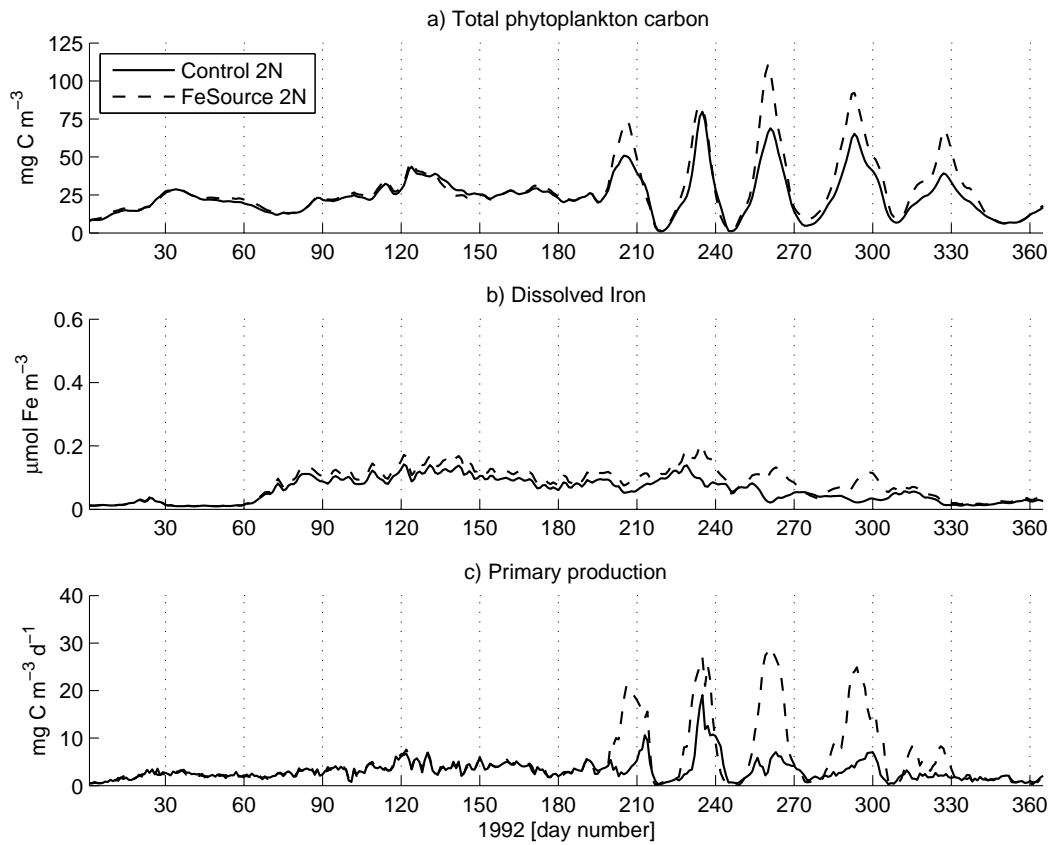
Figure 16. Same as in Fig. 15 but at 2°N, 120°W.